



1 **Hydraulic and geochemical impact of occasional saltwater intrusions**
2 **through a submarine spring in a karst and thermal aquifer (Balaruc**
3 **peninsula near Montpellier, France)**

4 Marie-Amélie Pétré^{1,2*}, Bernard Ladouche³, Jean-Luc Seidel¹, Romain Hemelsdaël⁴,
5 Véronique de Montety¹, Christelle Batiot-Guilhe¹, Claudine Lamotte³

6 ¹HydroSciences Montpellier, Montpellier University, CNRS, IRD, Montpellier, France

7 ²Now at North Carolina State University, Marine, Earth, and Atmospheric Sciences Department,
8 Raleigh, NC 27695, United States

9 ³BRGM, Montpellier University, Montpellier, France

10 ⁴Geosciences Montpellier, Montpellier University, CNRS, Montpellier, France

11

12 *corresponding author: Marie-Amélie Pétré, marieamelie.petre@gmail.com

13

14 **Abstract**

15 Submarine springs are a common discharge feature of the karst aquifers along the
16 Mediterranean coast. In some instances, occasional and localized saltwater intrusions can occur
17 through the submarine spring and negatively impact the quality of the groundwater resource.
18 The hydraulic and geochemical behavior of a submarine spring discharging into the Thau
19 lagoon just offshore of the Balaruc peninsula near Montpellier, France has been characterized
20 to determine the impacts of such phenomena to better understand the dynamics of a regional
21 karst aquifer and improve its groundwater management. This work is based on both historical
22 and new hydrogeological and geochemical data, illustrating 6 occasional saltwater intrusion
23 events (from 1967 to 2014) in the Thau lagoon area (southern France).

24 Hydraulic perturbation of the aquifer is propagated instantly within the Balaruc-les-Bains
25 peninsula and reaches a distance of about 5 km upgradient within 9 days. Comparison of
26 hydraulic heads during seawater intrusion events in 2010 and 2014 indicates an aggravation of
27 the phenomenon with an increase in hydraulic head variations.

28 In contrast, isotopic tracers (⁸⁷Sr/⁸⁶Sr, D/H, ¹⁸O/¹⁶O,) and Rare Earth Elements (REE)
29 demonstrate that the geochemical impact of these inversac events is only observed at the local
30 scale, but is still perceptible several years after the event. For example, some of the thermal
31 wells had not recovered their initial geochemical state 20 and 40 months after the last two
32 inversac events (2010 and 2014, respectively), suggesting a geochemical legacy of this
33 phenomenon within the complex karst system. By contrast, an adjacent deep karst compartment



34 located south of the study area is not affected by the saltwater intrusion and is characterized by
35 distinctly different hydrodynamic behavior.

36 Overall, this work on occasional and localized saltwater intrusions constitutes a key step in
37 understanding the dynamics of this complex karstic and thermal aquifer and will support the
38 management of the groundwater resource.

39 **1. Introduction**

40 Submarine springs are common discharge features of karst systems along the Mediterranean
41 coast (Bakalowicz, 2014; Fleury, 2005; Fleury et al., 2007; Stieglitz et al., 2013). Water from
42 these springs can support economic development or be exploited for drinking water supply.

43 In certain instances, especially during periods of low discharge, flow can reverse and instead
44 intrude into the upgradient karst aquifer, causing an adverse impact on the quality of the
45 groundwater resource and the economic activities that depend on it (Arfib and Gilli, 2010;
46 Droge and Bidaux, 1986). This phenomenon, termed “*inversac*” in French (Gèse, 1987;
47 Pinault et al., 2004), was previously described by Albéric (2004) and Joigneaux et al. (2011) in
48 a related context of river backflooding into karst springs.

49 The factors responsible for initiating and terminating *inversac* events are not particularly well
50 understood and the recovery of carbonate aquifers after a seawater intrusion is poorly described
51 (Han et al., 2015). Yet, it is necessary to understand the mechanisms controlling this
52 phenomenon, as well as the long-term impact of occasional and localized saltwater intrusions,
53 to appropriately manage the groundwater resources of such karst systems.

54 In this context, a hydraulic and geochemical study was undertaken to characterize the
55 occasional and localized saltwater intrusions into the karst aquifer of the Thau basin. More
56 specifically, our study addressed the following questions: (i) What are the hydraulic and
57 geochemical conditions in the karstic aquifer during and after an *inversac* event? (ii) What are
58 the triggering factors contributing to the occurrence of the *inversac* event? (iii) To what extent
59 is the aquifer system able to recover from an *inversac* event and get back to its original
60 geochemical state? (iv) What are the implications in terms of groundwater resources
61 management?

62 The Thau hydrosystem in the Balaruc-les-Bains area is an example of a karst and thermal
63 aquifer affected by occasional saltwater intrusions through a submarine spring. This complex
64 hydrologic system has been described by Aquilina et al. (1997, 2002, 2003), Doerfliger et al.



65 (2001) and Ladouche et al. (2001). However, the causes and extent of the impact of the saltwater
66 intrusions here remain poorly understood. The karst and thermal water resources across the
67 Thau hydrosystem are exploited both for drinking water supply and spa activities. Balaruc-les-
68 bains (Fig.1) is the largest spa in France with 55,000 visitors annually. In the past, water from
69 the Vise submarine spring was diverted to the seashore and used for aquaculture activities.
70 Additionally, the Thau lagoon supports an extensive shellfish aquaculture and fishery. Thus,
71 the economic stakes are high in this area and water use conflict has the potential to arise between
72 stakeholders during dry conditions, as a consequence of an increase in water demand, and the
73 occurrence of occasional saltwater intrusions (Chu et al., 2014; La Jeunesse et al., 2015).
74 Indeed, the karst system has been affected by six inversac events through the Vise submarine
75 spring over the past 50 years (Table 1), five of which (1967,1983, 2008, 2010 and 2014) have
76 been documented and described (Ladouche et al., 2011, 2019; Ladouche and Lamotte, 2015).
77 Human activities, such as bauxite mining upstream from the Vise spring, and intervention on
78 the spring itself are thought to have contributed to the saltwater intrusions over the 1967-1993
79 period by drawing down the hydraulic head of the karst system. Historically, these inversac
80 events produced an increase in the water level and electrical conductivity at the observation
81 points (thermal well and spring) in the Balaruc peninsula. A better understanding of this
82 phenomenon is for local use purposes, but is also of strategic importance for water managers of
83 the Issanka karst spring, a major drinking water supply in the area.

84 The last two inversac events in 2010 and 2014 lasted seven and five months, respectively. The
85 2014 inversac event led to the permanent abandonment of the Cauvy spring which provided
86 drinking water to a local population of 30,000.

87

88

89

90

91

92

93

94



Date	Duration	Causal Factors	End of Episode
2014 (May-October)	5 months	Very low waters. No storm surge in the lagoon. Groundwater withdrawals	Temporary low water level in the lagoon combined with recharge in the karst aquifer
2010 (June-December)	7 months	Intermediate waters	Heavy rainfall
2008 (January-March)	3 months	Low waters and a pump test on thermal well F14	-
1993 (October)	24 days	Low waters. Human intervention on the submarine spring and pumping test on the Balaruc peninsula	Heavy rainfall
1984-1987 (May-February)	20 months	Low waters. Lagoon with high water level. Human intervention on the griffon of the submarine spring	Heavy rainfall
1967 (October) - 1969 (March)	17/18 months	Dry conditions. Bauxite mining at the Cambelliès site. Large pumping (up to 1000m ³ h ⁻¹), that lowered the water level to -20 m asl	Cessation of groundwater pumping

95

96 Table 1. Summary of the observed occasional saltwater intrusions (inversac events) in the karst
 97 and thermal aquifer of the Thau basin.

98 A multi-tracer approach was followed to better define the origin and contribution of the thermal,
 99 karst and saltwater end-members under different conditions. Water stable isotopes (D/H,
 100 ¹⁸O/¹⁶O) were used to quantify the contribution of the saltwater end-member, whereas strontium
 101 isotopes (⁸⁷Sr/⁸⁶Sr) were used to distinguish the origin of salinity (thermal or marine). Rare
 102 Earth Elements (REE) were used to establish the chemical signature of the thermal wells in a
 103 reference context and to evaluate the influence of the marine signature over time. Finally, the
 104 B- isotope signature (d¹¹B) was used to trace water-rock interaction initiated during inversac
 105 events.

106 2. Study Area and Geological Setting

107 The Balaruc peninsula is located along the Mediterranean coast of southernmost France, west
 108 of the city of Montpellier, (Fig. 1a). The karst aquifer of the peninsula lies within the Middle
 109 and Upper Jurassic carbonates that outcrop to the north in the Aumelas Causse and the Gardiole
 110 Massif. These Jurassic carbonates are buried under Miocene to Plio-Quaternary deposits in the
 111 eastern part of the Thau lagoon (Fig 1b). Karstification and burial of the main Jurassic aquifer
 112 are the result of the geological history of the region described below.

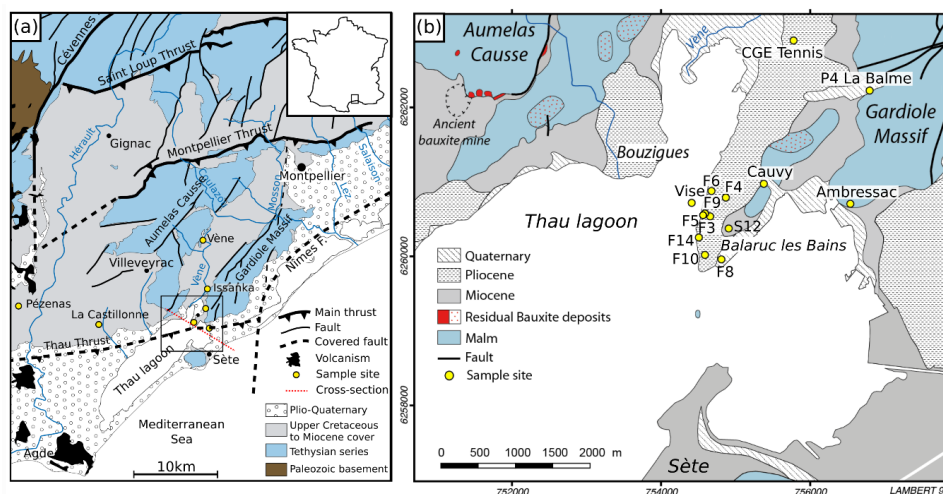


113 A Mesozoic series of Triassic to Early Cretaceous age was deposited during Tethyan rifting
114 (Baudrimont and Dubois, 1977; Debrand-Passard, 1984). The Mesozoic carbonate platform
115 underwent uplift during the Mid-Cretaceous, leading to exhumation that caused erosion of the
116 Early Cretaceous series and strong karstification of the Jurassic carbonates

117 The Mesozoic series was successively deformed during the Pyrenean collision phase from
118 Upper Cretaceous to Eocene time (Arthaud and Laurent, 1995; Arthaud and Seguret, 1981;
119 Choukroune et al., 1973; Choukroune and Mattauer, 1978) and the later rifting of the Gulf of
120 Lion (Arthaud et al., 1977; Arthaud and Seguret, 1981; Benedicto et al., 1996; Maerten and
121 Séranne, 1995; Séranne, 1999; Thaler, 1962). Then, the sea level rise of the Early Miocene
122 (Burdigalian) deposited transgressive sediments across the region (Fig. 1b). The overall
123 sedimentary record associated with these Upper Cretaceous to Middle Miocene geological
124 events, includes a wide range of detrital and carbonate facies deposited in marine, lacustrine
125 and fluvial environments (Combes, 1990; Marchand, 2019) (Fig. 1a).

126 The sea level fall related to the Messinian Salinity Crisis caused major river incision across
127 southern France which, as a consequence, deepened the karst system (Clauzon, 1982; Hsu,
128 1973; Ryan, 1976). The Messinian paleovalley in the coastal area was then flooded during the
129 early Pliocene when the Mediterranean was connected again to the Atlantic Ocean. Recent sea
130 level fluctuations over the last 5 Ma and associated Plio-Quaternary deposits have generated
131 the present day morphology of the Thau lagoon.

132 Structurally, the Balaruc-les-bains area is located between both the major NE-trending
133 Cevennes and Nîmes faults, to the south of the Pyrenean Montpellier Thrust (Fig. 1a). The study
134 area is also affected by the presence of the E-W oriented Pyrenean Thau Thrust. The complex
135 fault network at the intersection with the Nîmes Fault allows to bring the Paleozoic basement
136 at shallow depth (less than 2000 m according to borehole data) in the Balaruc-Sète area (Fig.
137 1a)



138

139 *Figure 1 (a) Simplified geological map showing the main structures of the Montpellier region. The box locates the*
140 *Balaruc-les-bains study area, between the Montpellier thrust and the Nîmes Fault. (b) Detailed geological map*
141 *of the eastern Thau lagoon. Sample sites indicated by the yellow dots in both maps correspond to the locations of*
142 *the thermal wells, karst springs, and other piezometric drilling sites. The location of the ancient bauxite mine*
143 *(Cambelliès) is indicated by the dashed oval in the northwest of the study area.*

144 3. Hydrogeological conceptual model of the Thau hydrosystem

145 The Balaruc peninsula is located at the point of natural convergence of different types of
146 waters including seawater from the Thau lagoon and Mediterranean Sea, cold karst
147 groundwater sourced from the Aumelas Causse and Gardiole Massif, and mineralized hot
148 thermal water rising from depth in the Balaruc peninsula (Aquilina et al, 2002). These different
149 types of water interact together in the Middle to Upper Jurassic carbonate reservoir. The
150 Montpellier Thrust to the north of the study area (Fig. 1a) brings impermeable marly Lias to
151 surface, which delimits the aquifer and acts as barrier to groundwater circulation. Groundwater
152 flow follows a general N-S trend from the Aumelas Causse and Gardiole Massif to the Balaruc
153 peninsula and the Mediterranean Sea. A clear hydraulic connection from the Vène spring
154 (Aumelas Causse) to Issanka spring (western slope of the Gardiole Massif) has been
155 demonstrated through artificial tracer testing (Paloc et Bonnet, 1969; Ladouche et al., 2001).
156 The main outlets of the Aumelas Causse karst network are the Vise submarine spring, the
157 Issanka spring and the Vène spring which acts as an overflow outlet. The Vise submarine spring
158 is located on the floor of the Thau lagoon at 30 m depth and constitutes the most downgradient
159 discharge feature of the hydrological system. The western part of the Gardiole Massif is drained
160 by the Vise spring as well as Cauvy and Ambressac springs.



161 At the regional scale, four levels of groundwater circulations have been recognized by previous
162 studies (Aquilina et al., 2003): 1) a surficial groundwater flow component originating from the
163 recharge areas that has a residence time <20 years; 2) an intermediate groundwater flow system
164 from the Aumelas Causse, that circulates below the Montbazin-Gigean basin and the Gardiole
165 Massif and discharges at points along the continental shelf (residence time of 50 years); 3) a
166 deep regional groundwater flow system directed from the Aumelas Causse to the Villeveyrac
167 Basin where several deep drillings (Pézenas and La Castillonne, depth of 1000 m) present hot
168 karstic waters with low mineralization (residence time of several thousand years); 4) a very
169 deep (>2 km) paleo-karst water circulation mixed with an ancient seawater circulation both
170 recharging the thermal reservoir that has residence times on the order of 100,000 years.

171

172 **4. Material and methods**

173 **4.1 Hydrogeological Monitoring**

174 Water level, specific electrical conductivity and temperature were measured at 10 locations on
175 an hourly basis during the last three inversac events in 2008, 2010 and 2014. The time-series
176 data used in this study come from the "national quantitative groundwater monitoring network
177 of the AFB/BRGM (available on the ADES website: <https://ades.eaufrance.fr> for P4 La Balme
178 (location 10166X0253) and CGE Tennis (location 10166X0212.) Other observation stations
179 (F5, F6, F8, F9 and S12) are managed by Balaruc-les-Bains and the municipality of Sète and
180 the Syndicat Mixte du bassin de Thau (El Cantou, F5-Issanka, Frescaly and Cauvy).

181 In order to compare the different inversac events, hydraulic head and electrical conductivity
182 were expressed with respect to reference values observed before the inversac events, as
183 discussed in the Results Section below. In Figures 3 and 5) b and 5d), the x-axis corresponds
184 to the number of hours elapsed since the beginning of the inversac event (t_0). The y-axis
185 represents the difference between the parameter (hydraulic head or electrical conductivity)
186 measured during the inversac and the preceding respective reference values. The variable "delta
187 H" is the difference between hydraulic head measured at time = "t" - hydraulic head observed
188 at time = t_0 (before the inversac event). Thus, a positive value corresponds to an increase
189 compared to the baseline condition and vice versa. This relative comparison permits the
190 evaluation of the inversac event perturbations with respect to the initial conditions prevailing
191 in the system and result in a more precise valuation of the transient states of the system.



192 4.2 Geochemical and Isotopic Analysis

193 Geochemical data for the 1996-2000 period are from Aquilina et al. (2002, 2003) and Ladouche
194 et al. (2001). They are considered as representative of reference geochemical conditions of the
195 karst system. Indeed, these data were collected three to seven years after the 1993 inversac,
196 which is considered as a sufficient time for the system to have returned to its equilibrium state
197 given the short, 21-day interval of this event.

198 New geochemical data (major ions and REE compositions) and isotope analyses (D/H, $^{18}\text{O}/^{16}\text{O}$,
199 ^3H , $^{87}\text{Sr}/^{86}\text{Sr}$ and d^{11}B) were determined for samples collected in October 2010, April and
200 September of 2012 and March and August of 2018, i.e. during the 2010 inversac, 17 and 22
201 months after the end of the 2010 inversac and 3.5 years after the end of the 2014 inversac.

202 Temperature, pH, Dissolved Oxygen and Electrical Conductivity ($T_{\text{ref}}=25\text{ }^{\circ}\text{C}$) were
203 measured in the field, using a portable pH meter, oxymeter and conductivity meter (WTW
204 3210).

205 Water sample for major and trace element analysis were filtered on-site with disposable PP
206 syringe with a $0.22\text{ }\mu\text{m}$ Durapore membrane and stored in acid washed HDPE bottles. Aliquots
207 for cations and trace elements were acidified to pH 2 with ultrapure HNO_3 (1% v/v). Samples
208 for H- and O-isotope analysis were collected in 15 mL amber glass vials capped with airtight
209 lids. One liter samples were collected for B- and Sr-isotope analysis in pre-cleaned HDPE
210 bottles and were later filtered in a cleanroom through a $0.22\text{ }\mu\text{m}$ Durapore membrane in a
211 pressurized Nalgene filtration unit, with samples for Sr-isotope analysis acidified with 1 %
212 ultrapure HNO_3 . Samples for tritium measurement were collected in 1 L HDPE bottles. All
213 samples were stored at $4\text{ }^{\circ}\text{C}$ before analysis. Chemical analyses were performed in the
214 HydroSciences Montpellier laboratory at the University of Montpellier. Total alkalinity was
215 measured by acid titration with 0.1N HCl. Major ion (Cl^- , NO_3^- , SO_4^{2-} , Ca^{2+} , Mg^{2+} , Na^+ , and
216 K^+) were analyzed by ion chromatography (ICS 1000 Dionex®). Precision error was $< \pm 5\%$.
217 After acidification with 1% HNO_3^- , trace elements (Li, B, Sr, REE and U) were analyzed by
218 inductively-coupled mass spectrometry using a Thermo Scientific® iCAP Q at the AETE-ISO
219 technical platform of the OSU OREME at the University of Montpellier. The use of an in-line
220 Argon Gas Dilution system permits the direct injection of highly mineralized samples without
221 prior dilution. Precision error was typically $< 5\%$. Fresh water reference material SLRS-6, and
222 seawater reference materials CASS-6 and NASS-6 for trace metals (National Research Council,
223 Canada) were analyzed every 20 samples to monitor analytical accuracy. Mean results are



224 within the range of certified uncertainties. Precision error for all analyses was typically <5%.
225 The REE data are represented in profiles, after normalization to a reference geological material,
226 the North American Shale Composite (NASC) for natural waters, which corresponds to an
227 average sample of North American shales (Taylor and McLennan, 1985).

228 For stable isotopes analysis, samples collected in 2010 were analyzed at BRGM Laboratories
229 using a Finnigan MAT 252 mass spectrometer, whereas those collected in 2012 and 2018 were
230 measured on an Elementar Isoprime stable isotope mass spectrometer at the LAMA laboratory
231 of HydroSciences Montpellier at the University of Montpellier. Calibration was performed by
232 repeated analyses of in-house standards of known isotopic composition in alternation with
233 samples. Oxygen ($^{18}\text{O}/^{16}\text{O}$) and hydrogen (D/H) isotope ratio measurements are expressed in
234 parts per thousand (i.e. ‰) in the familiar δ notation relative to the Vienna Standard Mean
235 Ocean Water (SMOW) standard, where $\delta = ([R_{\text{sample}}/R_{\text{standard}} - 1] \times 1000)$. Samples analyzed by
236 BRGM have a precision of ± 0.8 ‰ for δD values and ± 0.1 ‰ for $\delta^{18}\text{O}$ values, whereas those
237 determined at the University of Montpellier have an overall precision of ± 0.6 ‰ for both δD
238 and $\delta^{18}\text{O}$ values. Tritium analyses were performed at Hydrogeology laboratory at the Avignon
239 and Pays du Vaucluse University.

240 Sr-isotope analyses were made by thermal ionization mass spectrometry, at the BRGM
241 Laboratories for the 2010 samples and at the Centre de Recherches Pétrographiques et
242 Géochimiques in Nancy for the 2012 samples. Chemical separation of Sr was done using a Sr-
243 Spec ion-exchange column that has a total blank <0.5 ng for the entire chemical separation
244 procedure. Around 150 ng of purified Sr was loaded onto a tungsten filament and analyzed with
245 an average internal precision of $\pm 10 \cdot 10^{-6}$ (2σ) using a Finnigan MAT262 multiple collector
246 thermal ionization mass spectrometer. Measured $^{87}\text{Sr}/^{86}\text{Sr}$ ratios were normalized to a $^{86}\text{Sr}/^{88}\text{Sr}$
247 ratio of 0.1194. The reproducibility of $^{87}\text{Sr}/^{86}\text{Sr}$ ratio measurements was tested through replicate
248 analyses of the NBS987 standard (0.710240) for which the mean value was $0.710232 \pm 22 \times 10^{-6}$
249 at the BRGM and $0.710262 \pm 13 \times 10^{-6}$ at the CRPG.

250 Boron isotopic ratios were measured with a Neptune+, Thermo Electron inductively-coupled
251 mass spectrometer (at the BRGM laboratories for samples collected in 2010 (Guerrot et al.,
252 2011) and at the AETE-ISO technical platform of the OSU OREME at University of
253 Montpellier for the other samples. The average value determined for the NIST SRM 951
254 standard was 4.67 ± 0.0033 .

255



256 5. Results

257 5.1 Revised Conceptual Model for the Thau hydrosystem

258 The conceptual hydrogeological model of the Thau system at the local scale of the Balaruc-les-
259 Bains peninsula, is summarized in Figure 2. Thermal waters rise from the deep reservoir along
260 inferred faults in the vicinity of the Balaruc peninsula to reach the top of the Jurassic aquifer.
261 Consistent with the recent data compilation and results acquired in the Balaruc-les-Bains area
262 by the Dem'eaux Thau project (Ladouche et al., 2019), we propose that the Thau Thrust is
263 likely to provide the main pathway for thermal water. The karst freshwater is found below this
264 thermal lens as these cold waters are more dense. The diffuse intrusion of marine waters from
265 the Mediterranean Sea into the Jurassic limestone corresponds to a saltwater wedge and is
266 located below the karst waters which have a lower density. This saltwater wedge can
267 nevertheless have a more complex geometry than that represented in Fig. 2, since this
268 heterogeneous karst system is made up of multiple compartments. These contrasts in water
269 density generate several hydraulic interfaces that change according to the different hydraulic
270 heads resulting from continually- varying lagoon water levels, groundwater withdrawals and
271 recharge from precipitation.

272

Linear depth (m)	EC (mS cm ⁻¹)	Temperature (°C)
85	16.5	25
145	1	23
223	1	37
237	1	37
249	2	37
297	3.2	37
389	35	37

273

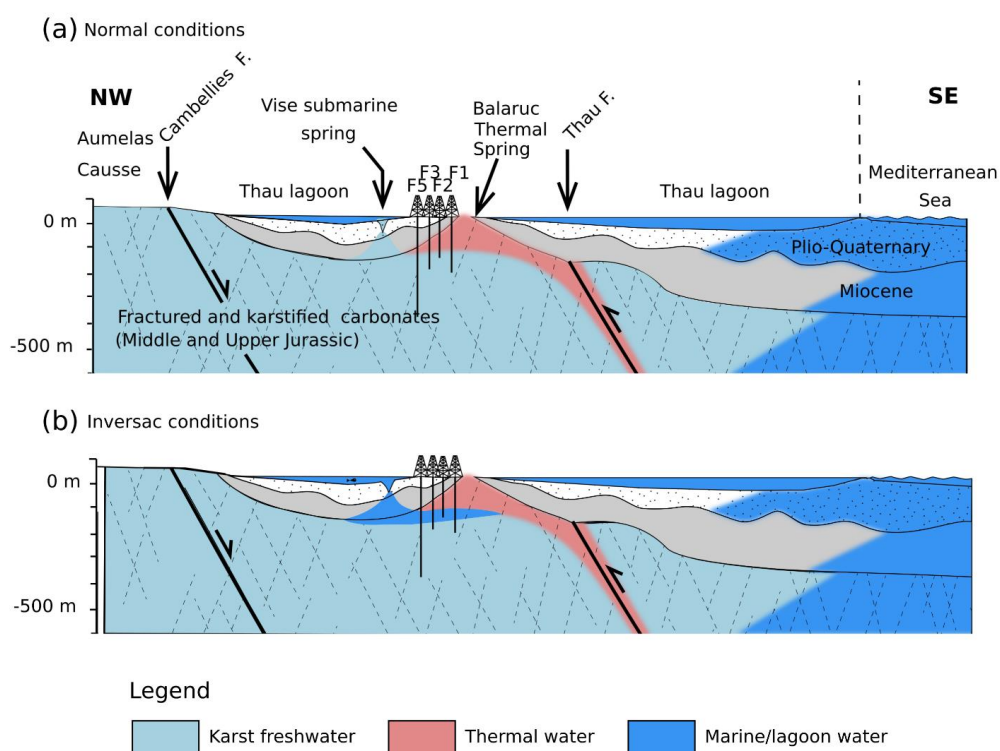
274 **Table 2 Water temperature and electrical conductivity from the exploratory drilling F13**
275 **at different depths. This inclined well (40°NW, N320°) is located near the F14 well (Fig.1b)**

276 This hydrogeological setting illustrated in Figure 2 was confirmed by the F13 exploratory well
277 (Table 2), that displayed contrasting electrical conductivity and temperature over depth.

278 Under normal hydrologic conditions (Fig. 2a), groundwater from the karst aquifer discharges
279 into the Vise spring, creating a plume of freshwater in the lagoon. During an occasional episode



280 of saltwater intrusion (or “inversac” event), the natural flow is reversed and saltwater from the
281 Thau lagoon flows into the Vise spring and enters the karstic aquifer via the Miocene cover
282 (Fig. 2b). The equilibrium between the different water bodies inside the Jurassic reservoir is
283 then strongly disrupted and the outflow of the karstic system through the Vise spring is
284 prevented. The characteristics of the thermal and karstic wells and spring in the Balaruc-les-
285 Bains peninsula are shown in Table 3



286

287 *Figure 2: Conceptual cross-section oriented NW-SE passing through thermal wells of the Balaruc peninsula, and*
288 *showing groundwater flows of the karst hydrosystem under (a) normal conditions and (b) inversac conditions.*
289 *Location of the cross-section is indicated in Figure 1a.*

290

291

292

293

294



Name and BRGM location reference number	Main water type	Well depth (m)	Depth to the top of the karst aquifer (m)	Distance from the Vise submarine spring (m)
F5 (10165X0185)	Thermal	105	-72	325
F6 (10165X0251)	Karst/thermal	63.5	-58.5	330
F9 (10165X0252)	Thermal	120	-88	375
F3 (10165X0183)	Thermal	175	-65	380
F4 (10165X0184)	Thermal	55	-38	460
F14 (10165X0257)	Thermal	300	-170	585
F8 (10165X0234)	Thermal	407	-136	930
Cauvy spring(10165X0021)	Karst	0	0 (outcrop)	1000
CGE Tennis (10166X0212)	Karst	115	-95	2600
P4 La Balme (10166X0253)	Karst	100	0 (outcrop)	2800
Frescaly (10162X0194)	Karst	54	-22	3400
F7-Issanka (10162X0184)	Karst	58	-12	4000
F5-Issanka (10162X0136)	Karst	27	-14	4450
El Cantou (10162X0197)	Karst			4535

295

296 **Table 3 Characteristics of the main wells and springs in the study area**

297

298 **5.2 Hydraulic impact of the inversac event**

299 This section provides a detailed hydrodynamic analysis of the most recent inversac event in
 300 2014 and then makes a comparison between the last three inversac events of 2008, 2010, and
 301 2014.

302 The hydraulic impact of the inversac event of 2014 was observed at all Balaruc peninsula
 303 springs and observation wells (Fig.3). From the first hours after the intrusion of lagoon water,
 304 a sharp increase in water level is observed for both karst and thermal wells, although the impact
 305 is variable for different locations. The hydraulic impact was most significant for thermal well



306 F9, for which a +2.2 m increase in hydraulic head was observed during the first four days of
307 the inversac event. The magnitude of the hydraulic impact is similar for F5 and F6 wells, with
308 experienced respective increases in hydraulic head of +1.8 m and +1.9 m respectively. A lower
309 increase in hydraulic head of just +0.7 m during the first four days of the inversac event was
310 recorded at the Cauvy spring, situated only 1 km from the Vise submarine spring. For this
311 spring, the increase is also partly caused by the interruption of water pumping. The hydraulic
312 disturbance gradually increases over a 3-months period for the CGE Tennis and P4 La Balme
313 wells, reaching a maximum of 2 m at CGE and around 1 m at P4 La Balme piezometers after
314 1,500 h.

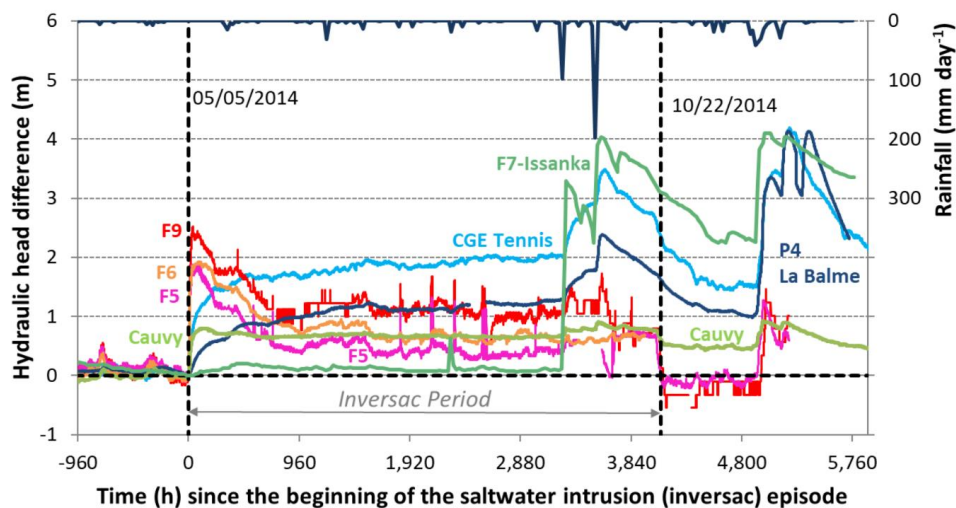
315 Two large rainfall events occurred in September and October 2014, some 3,400 h after the
316 beginning of the inversac event. These resulted in recharge to the aquifer that caused a sharp
317 increase in well water levels of +1.3 m at CGE Tennis and +1 m, at P4 La Balme.

318 The end of the inversac event occurred in October during the normal recession period of the
319 groundwater levels across the region. The thermal wells experienced a rapid decrease of
320 hydraulic head, which contrasted with the slow decrease of water levels in the CGE Tennis, P4
321 La Balme and F7-Issanka wells. After the inversac event, the water levels in CGE Tennis, P4
322 La Balme and Cauvy spring were observed in an intermediate position between the maximum
323 inversac and reference levels. In addition, the analysis of the water levels in the Thau lagoon
324 by Ladouche and Lamotte (2015) indicates that the end of the 2014 inversac resulted from
325 strong Tramontane winds caused an abrupt decrease in the lagoon water level in the vicinity of
326 the Vise submarine spring. Thus, both a temporary condition of a low water level in the Thau
327 lagoon and high waters conditions in the karst aquifer following heavy rainfall events appear to
328 have contributed to the conclusion of the 2014 inversac event.

329 In the Villeveyrac Basin area, the evolution of piezometric levels during 2014 indicates that the
330 hydrology of this region was not affected by the inversac event (Ladouche and Lamotte, 2015).
331 The elevated piezometric level of some 70 m here compared to the Vène area (3 m) strongly
332 suggests a compartmentalization of the karst aquifer.

333

334



335

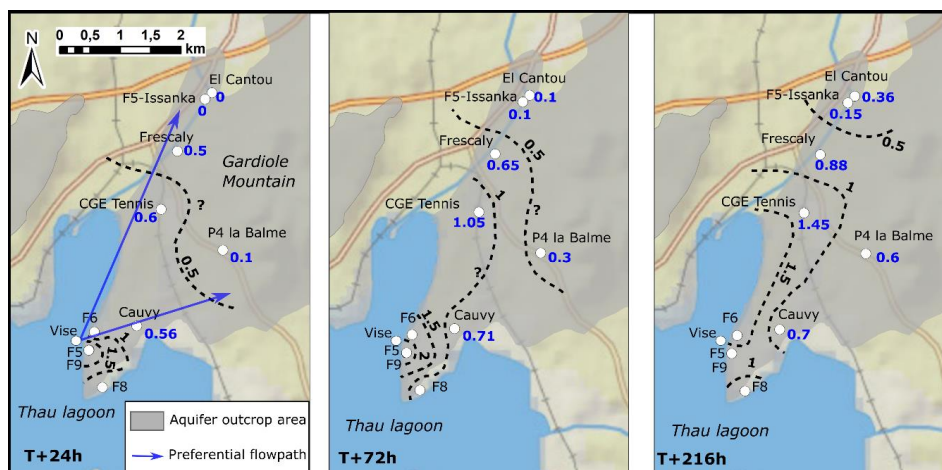
336 *Figure 3 Evolution of variations in hydraulic head (m) of wells and springs across the study area during the 2014*
337 *inversac event. The rainfall record during this time is shown at the top of the figure.*

338

339 Figure 4 illustrates the dynamics of the hydraulic disturbance to the karst system caused by the
340 2014 inversac event across the Balaruc-les-Bains peninsula. This detailed analysis demonstrates
341 the hydrologic connection between the Vise spring and the Issanka area. This perturbation
342 propagates rapidly and reaches a distance of 3 km upgradient in less than 24 h (i.e. a velocity
343 of 125 m h^{-1}). More specifically, the inversac causes an increase in hydraulic head of +1.5 m
344 throughout the peninsula and +0.5 m to the north of the peninsula (Frescaly, CGE Tennis) in
345 the first 24 h. This hydraulic perturbation then reaches the Issanka area in less than 72 h (i.e. a
346 velocity of 69 m h^{-1}) and causes a +0.4 m increase in hydraulic head within 10 days.

347 In addition, Fig.4 clearly shows that the hydraulic perturbation follows a preferential pathway
348 with a NNE orientation. A second minor flowpath follows a ENE orientation from the Vise
349 spring towards Cauvy and Ambressac springs.

350



351

352 *Figure 4 Spatial propagation of the hydraulic perturbation (hydraulic head increase in m) across the Balaruc-les-*
353 *Bains peninsula during the 2014 inversac event at three times after initiation: T+24 h, T+72 h, and T+216 h.*

354

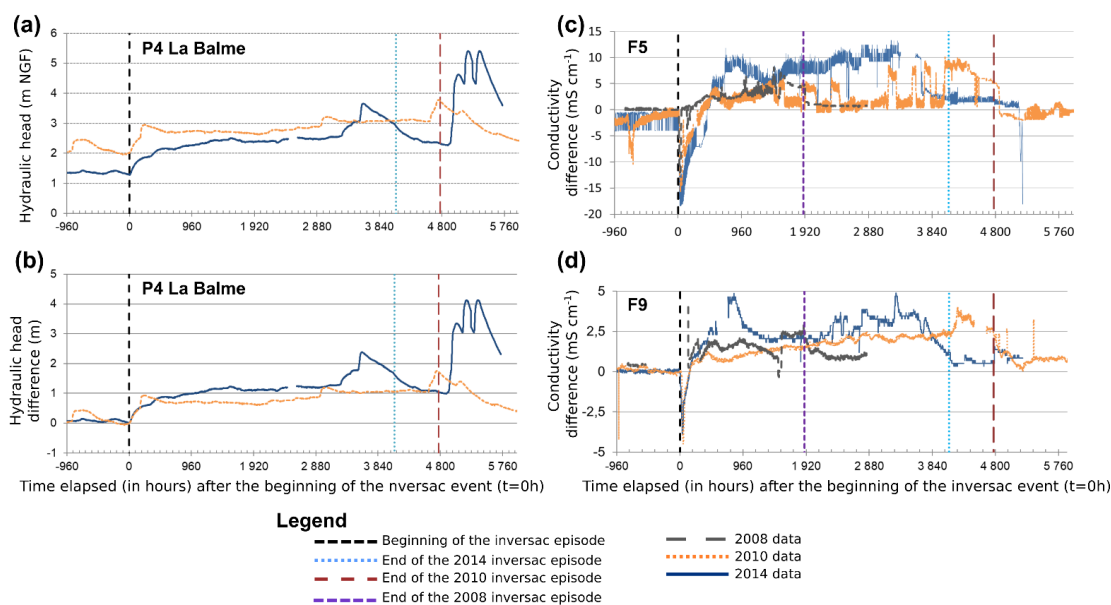
355 **Comparison between the 2008, 2010, and 2014 inversac events.**

356 Comparison between the last three inversac events of 2008, 2010, and 2014 provides a basis
357 for examining the hydraulic response to the phenomenon under different hydrological states.

358 The 2008 inversac caused an increase in the hydraulic heads of all the wells and piezometers in
359 the study area. For example, karst wells P4 La Balme and CGE Tennis showed respective
360 increases in the hydraulic head of +2 m and +1 m.

361 The increase in the water levels reached the same wells during the 2014 inversac as in 2008,
362 but was generally lower (more than 1 m for P4 La Balme and Frescaly and about 0.4 m in the
363 Issanka area).

364 In contrast to the 2008 and 2014 events, the hydraulic impact of the 2010 inversac did not reach
365 the Issanka area. An increase in hydraulic heads ranging from 1.5 to 2 m was only observed
366 north of the Balaruc-les-Bains peninsula for the P4 La Balme and CGE Tennis wells. The
367 explanation for this observation is discussed in the Discussion section.



368

369 *Figure 5 (a) Hydraulic head (m) and (b) hydraulic head variation (m) of the karst well P4 La Balme during the*
370 *2010 and 2014 inversac events; electrical conductivity variation (mS cm⁻¹) for the thermal wells (c) F5 and (d) F9*
371 *during the 2008, 2010 and 2014 inversac events.*

372 The hydraulic head of the karst well P4 La Balme was higher during the 2010 inversac
373 (intermediate waters) than during the 2014 inversac (very low waters) reflecting contrasted
374 hydrologic conditions during these periods (Fig.5 a). However, the hydraulic head difference,
375 with respect to the reference measured before the inversac (Fig. 5b), is higher in 2014 than in
376 2010. This suggests that the low water conditions magnify the hydraulic impact of inversac
377 events. Similarly, electrical conductivity differences for the thermal wells F5 (Fig. 5c) and F9
378 (Fig. 5d) show a stronger response to the 2014 inversac than during both the 2008 and 2010
379 inversacs.

380 5.3 Geochemical impact of the inversac event

381 In addition to the hydraulic impact just described, inversac events also have a notable
382 geochemical impact on the water bodies circulating within the karst system. As indicated in the
383 discussion of the “Hydrogeological conceptual model” section, the salty and highly mineralized
384 water of the lagoon mixes with thermal and karst waters to alter their quality. A multi-tracer
385 approach was undertaken to determine the long-term hydrochemical impact of inversac events
386 on the system that employed analysis of major ion contents, REE concentrations, and H-, O-,
387 Sr- and B-isotopic compositions. The geochemical analyses reflect contrasting conditions: the



388 1996-2000 reference interval, the 2010 inversac event, and the 2012 and 2018 post-inversac
389 period.

390

391 **Groundwater characteristics- Major ions and water types**

392 Outside of the Balaruc Peninsula, karst groundwater from Issanka spring and Pézenas deep
393 borehole (738 m) is of a Ca-Mg-HCO₃ type, characterized by electrical conductivity (EC)
394 values of about 500 $\mu\text{S cm}^{-1}$, in agreement with their karstic water type. The water from the
395 deep borehole has a higher temperature (37.2 °C) than that of the Issanka spring (about 17.5
396 °C).

397 Within the Balaruc peninsula, karst water from the Cauvy spring is of the same water type, but
398 displays elevated Cl contents and EC values of up to 222 mg L^{-1} and 1200 $\mu\text{S cm}^{-1}$, respectively.
399 In contrast, the thermal waters with temperatures that range up to 49.9°C are of a Na-Cl type
400 with Cl concentrations of up to 7,900 mg L^{-1} . The Ambressac spring, located east of the Balaruc
401 peninsula, is of mixed water type, with higher Cl concentration than at the Cauvy spring (up to
402 930 mg L^{-1}). Some samples also have high sulfate concentrations that approach 585 mg L^{-1} .

403 The Cauvy spring and the thermal wells F5, F6, and F9 were the most impacted by the 2010
404 inversac event, displaying a sharp increase of conductivity as well as high contents of Cl and
405 Na. For example, Cl concentrations in the Cauvy spring and F6 reached levels 8 to 11 times
406 above values typical of normal flow conditions (i.e. 1,240 mg L^{-1} compared with 157 mg L^{-1} for
407 Cauvy and 8611 mg L^{-1} compare with 759 mg L^{-1} for F6). For the Cauvy spring, which is used
408 for potable water, this Cl content observed during the inversac event far exceeds the drinking
409 water standard of 250 mg L^{-1} .

410 In a post-inversac context, Cl and Na concentrations observed for the Cauvy spring and F5, F6
411 and F9 wells in 2012 decreased significantly, with waters at these sampling points having
412 returned to levels close to those of the 1996-2000 reference period. By contrast, Cl
413 concentrations in wells F8 and F3 increased between 2010 and 2012, suggesting an increase in
414 the relative contribution of the marine water component.

415

416 **Karst water and saltwater mixing traced by water stable isotopes**

417 As shown in Figure 6a, different waters present in the Balaruc peninsula hydrosystem are
418 characterized by distinct δD and $\delta^{18}\text{O}$ values. Normal waters within the karst system lie close
419 to the Local Meteoric Water Line ($\delta\text{D} = 8 \delta^{18}\text{O} + 14$; Ladouche et al., 1998), illustrating their



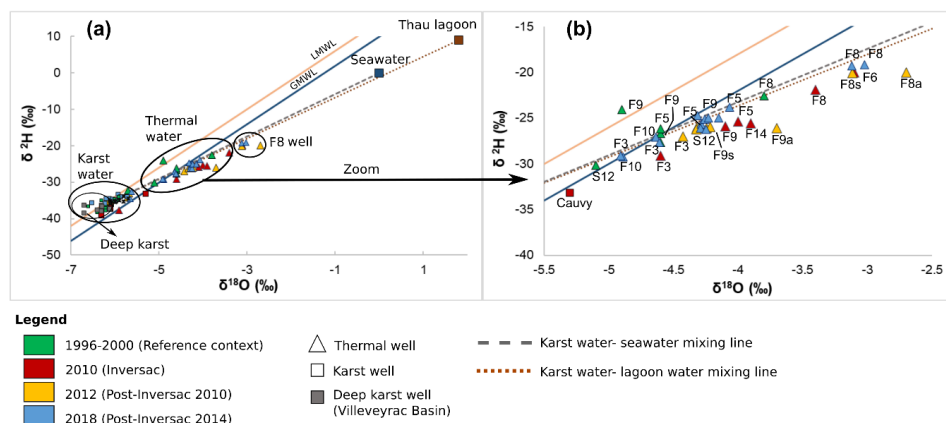
420 meteoric origin. Waters sampled from thermal wells are more enriched in D and ^{18}O than the
421 karst waters and are distributed along a karst-saltwater (i.e. lagoon or seawater) mixing line.

422 This result indicates that thermal waters result from a mixing between karst and marine end-
423 members. However, stable isotopes information alone does not allow a determination of the
424 origin of the marine end-member, which could be either lagoon water or modern or ancient
425 seawater. Samples from the F8 thermal well show a slightly enriched stable isotopes signature
426 compared to the other thermal wells, reflecting a greater contribution of the saltwater end-
427 member in this area, as initially indicated by Aquilina et al. (2002).

428 F6 samples from the reference period are located within the karst water domain, confirming the
429 strong influence of karst waters in this well (Aquilina et al. 2002) under normal flow conditions.

430 H- and O-isotopic signatures of groundwater from F5, F9, F8 and F6 thermal wells are shifted
431 towards the saltwater end-member during the 2010 inversac. Then, in 2012 and 2018, their δD
432 and $\delta^{18}\text{O}$ values decreased, but still remain in an intermediate position between the inversac
433 maximum and the reference (1996-2000) period minimum. This result raises the question of
434 the persistence of the chemical impact in the aquifer system following occasional saltwater
435 intrusions.

436 Thermal wells F14, F5 and the thermal spring S12 show similar mixing proportions for the
437 2012 and 2018 post-inversac times. For F5 and S12, these mixing proportions are intermediate
438 between that of the 2010 inversac event and the 1996-2000 reference time. Groundwater
439 samples of F3 well do not follow the same evolution, as the shift in its $\delta^{18}\text{O}$ value does not
440 appear inversac related (Fig. 6b).



441

442 *Figure 6 H- and O-isotopic compositions, expressed as δD and $\delta^{18}O$ values, of (a) karst waters, thermal waters,*
 443 *F8 well water, seawater, and Thau lagoon water, showing the Global Meteoric Water Line (GMWL) after Craig*
 444 *(1961) and the Local Meteoric Water Line (Ladouche et al., 1998) for reference; (b) expanded view of the thermal*
 445 *well water array from (a) during reference, inversac, and post-inversac conditions*

446

447 Two end-member mixing calculations were made to model the geochemical impact of the 2010
 448 inversac event on waters at the different sampling points across the study area, the first based
 449 on stable isotope ratios and the second using Cl concentrations measured in 2010, 2012, and
 450 2018. The proportions of karst water (f_{fresh}) and saltwater (f_{salt}) in a groundwater sample were
 451 calculated using the following formula:

$$452 \quad f_{salt} = \frac{C_{sample} - C_{fresh}}{C_{salt} - C_{fresh}} \quad \text{equation 1}$$

$$453 \quad f_{salt} + f_{fresh} = 1 \quad \text{equation 2}$$

454

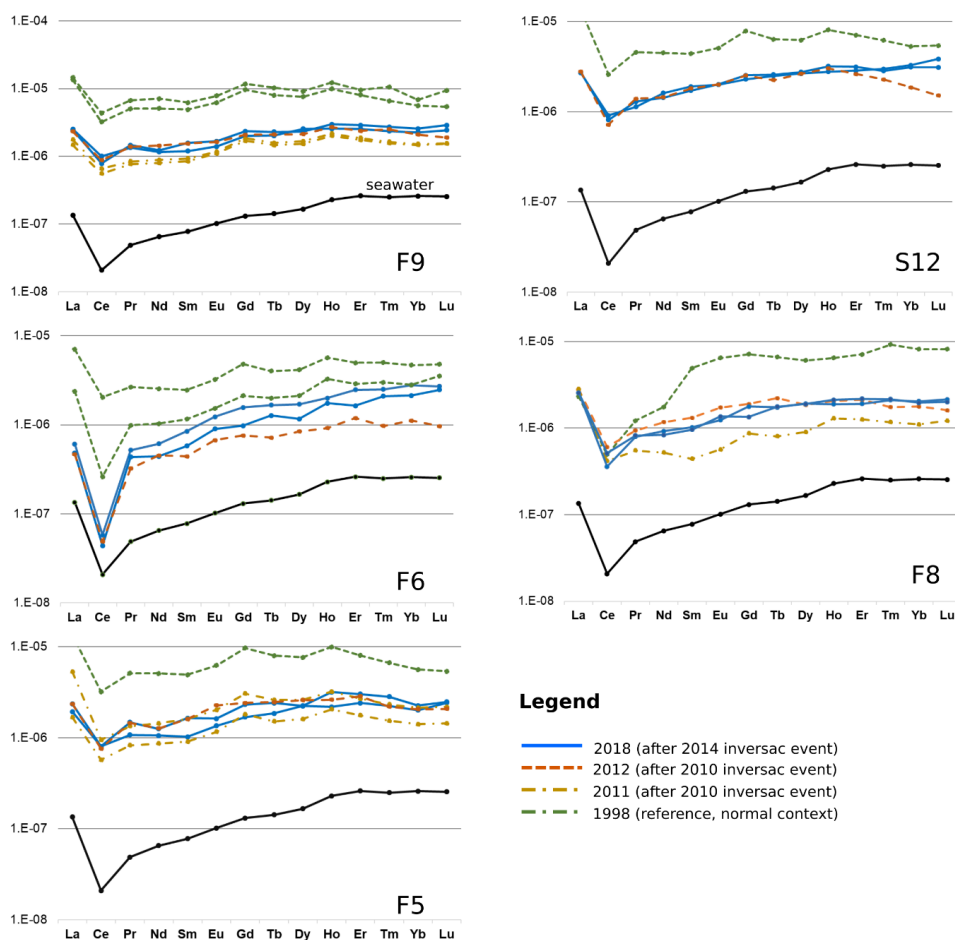
455 Results of the mixing calculations are included in the Supplement (Table S1). This calculation
 456 gives an indication of the magnitude of the karst water and saltwater component in of each
 457 water sample, but does not provide additional insight into the origin of groundwater salinity.
 458 The calculated fractions of saltwater for the karst wells and spring are similar for the three
 459 tracers ($\delta^{18}O$, δD and Cl). However, for thermal wells with typical high Cl contents, the
 460 fractions obtained are distinct for the different tracers, indicating another source of Cl for these
 461 wells. Indeed, as indicated by Aquilina et al. (2002), Cl in the thermal wells is thought to derive
 462 from both seawater and the thermal water end-member, which is itself partly constituted of old
 463 seawater.



464 **Inversac persistence revealed by REE**

465 The 14 members of the lanthanide group of elements (from La to Lu), commonly termed rare
466 earth elements (REE), constitute an effective tool to trace water origin, water/rock interaction
467 and mixing processes (Johannesson et al. 1997, Tweed et al. 2006, Zhan et al. 2013, Gil et al.
468 2018). The REE are naturally present in natural waters at trace concentrations and their
469 normalized abundances, represented as a distribution pattern of individual REE ordered by their
470 atomic number, provide a means of visualizing the behaviour of the entire group of elements.

471 The REE profiles for seawater and groundwater from the thermal wells (S12, F8, F9, F5, F6)
472 and seawater are shown in Figure 7 for the pre-inversac reference and three post-inversac
473 situations (Fig. 7). With the exception of the F6 well, all patterns are generally flat and show a
474 small negative Ce anomaly. The F6 profile exhibits a more pronounced Ce anomaly and an
475 enrichment in heavy REE. These characteristics are those of limestone REE profiles, inherited
476 from the seawater REE profile and confirm the strong karst influence of F6 samples.



477

478 *Figure 7 REE profiles for thermal wells at different times: the 1998 data are for the pre-inversac reference state,*
 479 *whereas the 2011, 2012 and 2018 profiles are for the three post-inversac situations.*

480

481 REE contents during the 2011-2012 post-inversac period were generally lower than for the 1998
 482 reference context. This is to say that, REE profiles in a post-inversac context lie in an
 483 intermediate position between the seawater profile and the reference profiles. Such an
 484 observation indicates that the thermal wells, at the time of sampling 20 months later in 2012,
 485 were still under the influence of the perturbations caused by the 2010 inversac event. The post-
 486 inversac profiles for 2012 and 2018 are quite similar, except for the F6 well, suggesting a
 487 similarity in extent of the 2010 and 2014 inversac events and post-event response of the
 488 hydrologic system. The REE profile for the F8 thermal well displays a distinctly different
 489 evolution, with an increasing shift away from the seawater profile over time. However, this well



490 is not hydraulically impacted by the occasional saltwater intrusion. The observed evolution does
491 not seem related to an increase in water withdrawals, but may instead reflect a relative decrease
492 in the contribution of thermal component over time.

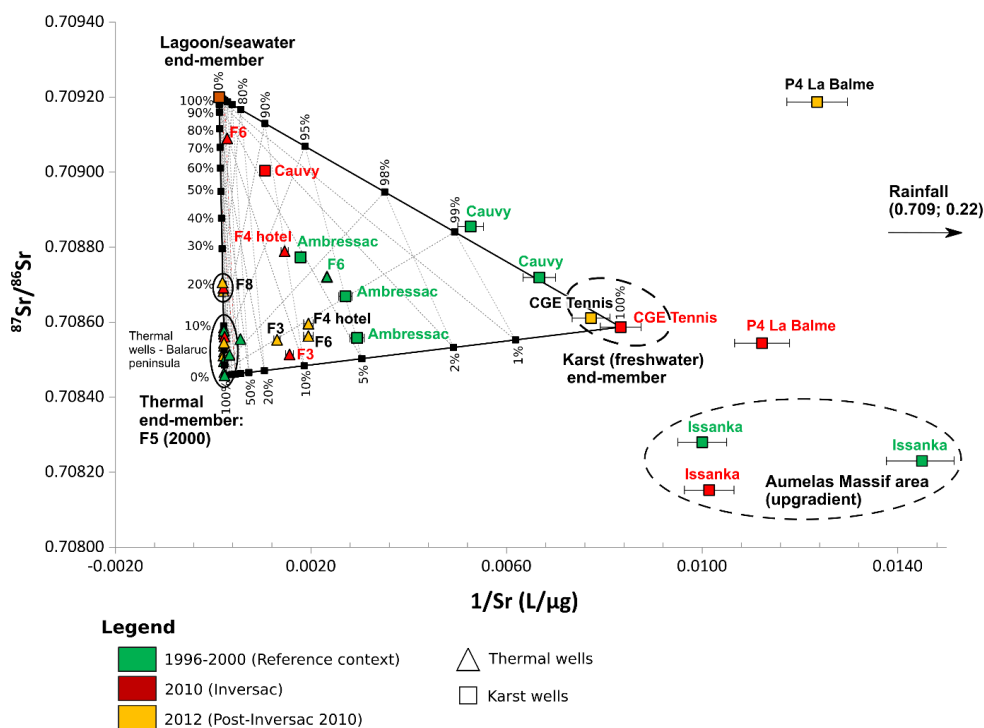
493 **Characterization of the thermal and marine contributions from the strontium isotope**
494 **ratios $^{87}\text{Sr}/^{86}\text{Sr}$**

495 Consideration of strontium geochemistry allow the characterization of the thermal and marine
496 water contributions to the karst groundwaters. Sr-isotope ratios ($^{87}\text{Sr}/^{86}\text{Sr}$) for the groundwater
497 and lagoon samples are plotted as a function of strontium in Figure 8, where the 2010 and 2012
498 post-inversac data are compared with the 1996-2000 reference situation. It was assumed that
499 the waters from the F5 thermal well in the Balaruc peninsula during the reference interval are
500 representative of the thermal end-member, which is not affected by the karst or marine waters.
501 It is notable of the Sr-isotopic signature and Sr content of the CGE Tennis samples are relatively
502 stable in all contexts and fully representative of karst waters under confined conditions. The
503 Thau lagoon water sample is compositionally similar to that of the Mediterranean Sea and
504 corresponds to the saltwater end-member. The $^{87}\text{Sr}/^{86}\text{Sr}$ isotopic signature of karst waters and
505 thermal end-member are similar, indicative of derivation through water-rock interaction with
506 the Mesozoic carbonate aquifer. The karst end-member is different from the thermal end-
507 member by its lower Sr concentrations ($100 \mu\text{g L}^{-1}$), suggesting different water residence times.

508 As shown in Fig.8, all water samples plot within a ternary domain, confirming that the
509 geochemistry from the Balaruc peninsula groundwater can be explained by a 3-member mixing.
510 The karst waters from the Issanka spring that drain the Aumelas Massif have a lower $^{87}\text{Sr}/^{86}\text{Sr}$
511 ratios and Sr contents. The Issanka isotopic signature defines an up-gradient end-member for
512 the karst system, unaffected by mixings of the thermal and seawater that characterizes the
513 Balaruc peninsula. Waters from the P4 La Balme piezometer had a very high $^{87}\text{Sr}/^{86}\text{Sr}$ ratio in
514 2012, almost certainly reflecting the influence of rainfall infiltration since this sample site is
515 located at the outcrop of the aquifer and may be representative of surficial recharge water to the
516 karst aquifer.



517



518

519 *Figure 8 Plot of $^{87}\text{Sr}/^{86}\text{Sr}$ ratio versus Sr concentration (as $1/\text{Sr}$) for springs and wells of the Balaruc peninsula*
 520 *for different hydrogeological situations: pre-inversac reference (green), 2010 inversac (red) and 2012 post-*
 521 *inversac (yellow).*

522

523 The contribution of each end-member (saltwater, thermal water and karst water) to groundwater
 524 samples under different hydrogeological situations related to inversac events were estimated
 525 through 3-component mass balance equations following Faure (1986):

$$526 \quad f_{\text{salt}} + f_{\text{karst}} + f_{\text{therm}} = 1 \quad \text{equation 3}$$

527 where:

$$528 \quad (^{87}\text{Sr}/^{86}\text{Sr}) \cdot [\text{Sr}]_{\text{sample}} = f_{\text{salt}} (^{87}\text{Sr}/^{86}\text{Sr}) \cdot [\text{Sr}]_{\text{salt}} + f_{\text{karst}} (^{87}\text{Sr}/^{86}\text{Sr}) \cdot [\text{Sr}]_{\text{karst}} + f_{\text{therm}} (^{87}\text{Sr}/^{86}\text{Sr}) \cdot [\text{Sr}]_{\text{therm}}$$

529 Results of the mixing calculations are in the Supplement (Table S2).

530 The Sr-isotopic composition of the Cauvy spring is quite variable during the reference interval,
 531 with samples aligned along the karst-saltwater mixing line in Figure 8. The contribution of the
 532 saltwater end-member to the spring discharge is negligible under normal flow conditions, with



533 the Cauvy isotopic signature very close (99%) to the karst end-member. However, the Cauvy
534 spring is strongly impacted by the inversac phenomenon. Although the karst end-member
535 remains dominant at 88.1 ± 0.2 %, the contribution of saltwater end-member increases to $8.1 \pm$
536 0.5 % and that of the thermal end-member reaches about 3.8 ± 0.3 % during the 2010 inversac
537 event. The contribution of thermal waters to the Cauvy spring is not surprising, as it is located
538 close to the old thermal spring (S12), but the large contribution of the saltwater end-member
539 during inversac events implies a preferential groundwater flow axis between the spring and the
540 Vise submarine spring. Pinault et al. (2004) have shown that variations in the contribution of
541 thermal waters may be related to the existence of a piston effect on the thermal reservoir,
542 particularly following an intense recharge event.

543 Thermal well waters of the Balaruc peninsula are all aligned along the thermal-saltwater end-
544 member mixing line in Figure 8, except for F3, F4 hotel, and F6 waters, each of which
545 documents a significant contribution from the karst end-member (87.9 ± 0.3 %, 89.8 ± 0.2 %
546 and 53.7 ± 0.6 %, respectively).

547 The evolution of the isotopic signature for the F5, F9 and F14 borehole waters shows a similar
548 pattern. Thermal water $^{87}\text{Sr}/^{86}\text{Sr}$ ratios increase during the 2010 inversac event, but then
549 decreases in 2012 to values intermediate between the inversac condition and normal state. These
550 observations suggest that waters from this group of thermal wells were strongly affected by the
551 2010 inversac had not returned to their 1996-2000 pre-inversac Sr-isotope signature by the 2012
552 post-inversac situation.

553 The contribution of the Thau Lagoon end-member increased to 8.3 ± 1.3 % for the F9 waters
554 during the 2010 inversac, the thermal end-member was 91.3 ± 0.6 %, the karstic contribution
555 being negligible (0.4 ± 1.9 %). The contribution of the Thau lagoon end-member decreased to
556 5.7 ± 1.2 % during the 2012 context.

557 Reporting on water collected from the F8 borehole, Aquilina et al. (2002) noted a seawater
558 contribution to the thermal waters in this area of the Balaruc peninsula, which we have
559 estimated to be 8.8 ± 1.3 % for the 1996-2000 pre-inversac reference period.

560 The strontium concentrations and $^{87}\text{Sr}/^{86}\text{Sr}$ ratios of F8 well waters were very similar in 2010
561 and in April and September of 2012. Although the contribution from the saltwater end-member
562 during the 2010 inversac was greater than the reference condition (18.0 ± 1.6 % instead of 8.8
563 ± 1.3 %), and remained between 17.5 ± 1.6 % to 21.2 ± 1.8 % from April to September 2012.

564 The thermal well F8 does not seem to be impacted by a direct intrusion of lagoon water during
565 the inversac event but instead influenced by seawater already within the hydrosystem.



566 Water at the F6 borehole was the most impacted by the 2010 inversac. During this time, the
567 contribution from the saltwater end-member sharply increased from 1.6 ± 0.1 % to 35.4 ± 1.8
568 % between 1996 to 2010 then decreased to 0.6 ± 0.1 % in 2012, a value below the 1996 to 2000
569 reference interval. Waters from the F6 borehole are representative of the upper part of the
570 Jurassic aquifer and demonstrate a significant contribution of the karst end-member (94.1 ± 0.1
571 % to 91.2 ± 0.2 % in 1996 and 2012). This karst contribution remains significant during an
572 inversac context (53.7 ± 0.6 %). Thus, waters from the F6 well illustrate the range of
573 fluctuations of the thermal component.

574 By contrast to the F6 well, the three end-member contributions are relatively stable for the
575 waters of Ambressac spring. Indeed, water samples display a large variability, with a saltwater
576 end-member contribution of between 1.1 ± 0.1 % and 2.7 ± 0.2 % and a karst contribution
577 between 94.4 ± 0.1 % and 91.5 ± 0.1 % over the reference interval (1996-2000). The thermal
578 contribution ranges between 4.4 ± 0.1 % and 5.8 ± 0.2 % during normal times.

579

580 **Boron Isotope Tracking of Water-rock interactions**

581 A lack of knowledge of the baseline B-isotopic signature during normal flow conditions does
582 not allow to discuss the origin of boron and its quantification for thermal borehole waters.

583 However, examination of $\delta^{11}\text{B}$ variations as a function of B/Cl ratio clearly identifies water
584 interactions with clay minerals. Indeed, boron is present in aqueous solution, in the form of
585 boric acid $\text{B}(\text{OH})_3$ and borate ions $\text{B}(\text{OH})_4^-$. The distribution between these two species depends
586 on pH, temperature and salinity (Hershey et al 1986, Hakihana 1977). For the boron isotopes,
587 ^{11}B is preferentially incorporated into boric acid whereas ^{10}B has a greater affinity for the borate
588 ion. During the water-rock interaction, $\text{B}(\text{OH})_4^-$ will be preferentially adsorbed onto clay
589 minerals or organic matter, resulting in a decrease of water B concentration and a consequent
590 enrichment of ^{11}B in residual water.

591 Figure 9 shows the Cl/B ratio as a function of B isotopic composition. $\delta^{11}\text{B}$ of the Thau Lagoon
592 is 39.1 ‰, in agreement with the signature of the modern seawater of 39.5 ‰; (Aggarwal et al.,
593 2004, Aggarwal and Palmer 1995). By contrast, karst waters display a range of $\delta^{11}\text{B}$ values
594 from 23.1 to 52.3 ‰, but are strongly ^{10}B enriched relative to seawater signature, whereas,
595 thermal waters have $\delta^{11}\text{B}$ values of up to 44.3 ‰ that are similar to or higher than the seawater
596 signature.



617 *Figure 9. Plot of $\delta^{11}B$ versus Cl/B ratio for different hydrogeological contexts: 2010 (inversac times in red),*
618 *2012 and 2018 (post-inversac times in yellow and blue)*
619

620 **6. Discussion**

621 **6.1 Implications for Dynamics of the Thau hydrosystem**

622 **Extent of the hydraulic impact and conditions required to reach the upgradient area of** 623 **Issanka**

624 Analysis of the hydraulic response of the Thau hydrosystem to the last inversac events provides
625 insights into the dynamics of the system and a better understanding of the underlying controlling
626 mechanisms. For example, the 2010 inversac did not impact the upgradient area of Issanka in
627 contrast to the 2008 and 2014 inversac events. This is attributed to the fact that the karst system
628 in 2010 was less in deficit than at the time of the 2008 and 2014 events, when very low flow
629 conditions prevailed. For example, piezometric levels measured for the Issanka area in 2008
630 and 2014 were lower than in 2010 (i.e. 6.82 m in 2008 and, 6.89 m in 2014 and, 9.33 m in
631 2010). Considering that the overflow level of the Issanka spring is at ~9.5 m, this implies that
632 the hydraulic impact in the Issanka compartment is controlled by the pressure head difference
633 between the upstream (Issanka) and downstream (Balaruc peninsula) compartments.
634 Piezometric monitoring at these different times illustrates that the occurrence of the inversac
635 phenomenon is mainly determined by hydrogeological processes that occur within the
636 downstream compartment of the karst system. Water level of the Thau lagoon is one of the
637 controlling parameters. At inversac initiation in 2008, the water level in the Thau lagoon was
638 higher than in 2010 at 1 m compared to just 0.5 m, but then only of 0.2 m in 2014. For the
639 inversacs of 2008 and 2010, the sudden rise in lagoon waters of + 0.5 m and + 0.4 m,
640 respectively, in a few hours is considered to be
641 the triggering factor. By contrast, no sudden change in the water level of lagoon was observed
642 in 2014. The triggering mechanism of this event is still poorly understood, however it is likely
643 that the withdrawals from the aquifer for drinking water and irrigation purposes as well as the
644 low recharge during the previous winter may be the explanatory factors.

645 Thus, two factors would need to be combined for an inversac to reach the upgradient area of
646 Issanka: (i) first, low water conditions that produces a very low hydraulic head throughout the
647 aquifer. The hydraulic head would need to be lower than 7 m in the Issanka area, i.e. below
648 than the hydraulic head imposed by the saltwater intrusion; (ii) an event-specific triggering



649 mechanism, such as a sudden rise in the water level of the Thau lagoon or groundwater
650 withdrawals.

651 The intrusion of lagoon waters in the system causes a 2-phase response within the Thau
652 hydrosystem:

653 1) A short initial transient phase of a few days duration during which there is a
654 reorganization or displacement of the different karst, thermal and marine water bodies
655 within the hydrosystem,

656 2) A longer transient phase during which the hydrosystem reaches a new equilibrium (in
657 30 days in 2008 and 2010, 40 days in 2014) with clear evidence of water mixing causing
658 important changes in the physico-chemical parameters of waters from the sampling
659 points F5, F6, F9 and the Cauvy spring.

660

661 **The impact on water quality is local whereas the hydraulic impact is perceived at the**
662 **regional scale**

663 Results in section 5.1 showed that the hydraulic impact of an inversac event is instantly
664 propagated throughout the Balaruc peninsula and the effects of such events can also reach
665 longer distances into the karst system than previously described. The return to the equilibrium
666 situation occurs within days after a significant recharge event and is much more rapid than the
667 dissipation of the chemical impact of the inversac event. Indeed, the 2010 and 2014 inversac
668 events lasted about 6 months and had a persistent chemical impact on the hydrosystem. It stayed
669 perceptible on the quality of the water in certain compartments from 20 months to 42 months
670 after the occasional inversac intrusions ceased.

671 Even though the geochemical conditions within the hydrosystem were not monitored during
672 the 2014 inversac event, the 2018 data are similar to those for 2012, suggesting that the
673 hydrosystem did not reach its geochemical reference conditions and was still under a state of
674 influence by the latest inversac event.

675 Geochemical analysis indicates that the 2010 inversac had the greatest impact on waters from
676 the F6 well and the Cauvy spring, thus confirming the existence of a preferential groundwater
677 flowpath between the Vise spring and those points.

678 The physico-chemical disturbances resulting from inversac event are not observed at sampling
679 points CGE Tennis, P4 La Balme, Issanka located in the upgradient area of the Balaruc

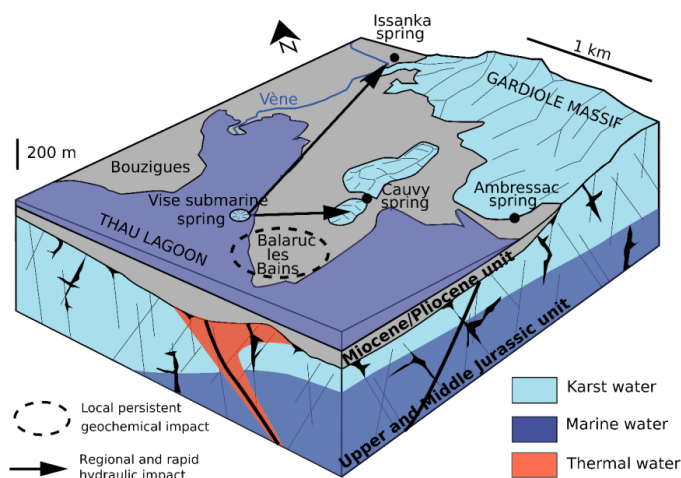


680 peninsula. The geochemical impact is, therefore, restricted to within a 1-kilometer radius from
681 the Vise spring (Fig. 10).

682 This slow geochemical recovery is best explained by the characteristic internal heterogeneity
683 of the karst aquifer, which is typically described in terms of a triple porosity model comprising:
684 (i) matrix or primary porosity, (ii) fracture porosity and (iii) conduit porosity (Palmer et al 1999;
685 Martin and Sreaton 2001). Influx of inversac water into the matrix porosity of the karst aquifer,
686 its storage, and then prolonged time of removal and return to fracture and conduit flow explains
687 the persistent fingerprint of the saltwater intrusions in the Balaruc peninsula.

688 Wells F8 and F10 in the southern part of the Balaruc peninsula were not affected by the inversac
689 events. This part of the hydrosystem corresponds to a deeper compartment in the karst system,
690 where the top of the Jurassic aquifer is 136 m deep in the F8 well and 195 m deep in the F10
691 well, which appears to be less hydraulically connected to the rest of the peninsula. Previous
692 studies postulated that an indirect impact of an inversac event might occur (Ladouche et al.,
693 2012). However, the increasing mineralization of F8 waters over time from 20 mS cm⁻¹ in 1996
694 to 26.5 mS cm⁻¹ in 2018 (Figure S1 in the Supplement) suggests that waters from this well are
695 not influenced by the occasional saltwater intrusions into the hydrosystem. This distinct
696 evolution cannot be explained by pumping withdrawals as well withdrawals rates in the F8
697 thermal well were steady over the period of inversac monitoring. However, a decrease in the
698 recharge rate from the karst system could result in an increase in the proportion of the thermal
699 or marine end-member contributions. Recent monitoring of springs (Ambressac and S12) will
700 address this question in the Dem'Eaux Thau project.

701 A comprehensive review of historical inversac events undertaken as part of this study showed
702 that there is a hydraulic connection between the Villeveyrac Basin and the Balaruc peninsula.
703 The relationship between these two regions is clearly demonstrated as dewatering of a bauxite
704 mine in the Cambelliès area (Fig.1) triggered the 1967 inversac event.



705

706 *Figure 10. Bloc diagram of the study area showing the spatial extent of the hydraulic and geochemical impacts.*

707 **6.2 Implications on groundwater management:**

708 Results presented here illustrates the fragile equilibrium that exists between different
709 groundwater bodies in the Thau hydrosystem. During low flow conditions, any modification of
710 the exploitation regime of the system can cause an inversac event and cause deleterious long-
711 term consequences.

712 Historically, the 1967 and 2010 inversac events led to the complete cessation of withdrawal
713 from the Cauvy spring, followed by its subsequent abandonment because the quality of this
714 major drinking water supply was strongly impacted by the inversac events.

715 The Issanka spring is another major source of drinking water in the area for a population of
716 40,000. This study recognized the conditions needed for the hydraulic impact of an inversac
717 event to reach the Issanka well-field. Such new understanding can support water management
718 operations by facilitating the prediction of the arrival of an inversac disturbance, using the
719 criteria highlighted in section 6.1.

720 While the southern compartment of the hydrosystem has not been impacted by inversac events,
721 the gradual increase in mineralization observed for the F8 thermal well has the potential to
722 affect its quality over time. In order to sustain the water quality of this thermal well, further
723 studies should investigate the specific dynamics of this karstic compartment and the underling
724 mechanism explaining this observation. More specifically, the hydraulic connection between
725 this deep compartment with the Sète thermal system south of the study area should be
726 investigated.



727 Finally, unlike classical saline intrusion, the inversac events mobilize sediments loaded with
728 organic matter during saltwater intrusions from the Vise spring. This intrusion of sediments
729 may have an additional impact on the water quality within the karstic hydrosystem as suggested
730 by B-isotopic signatures. Future studies could explore the fate and transport of the organic
731 matter in the karst system.

732

733 **7. Conclusion**

734 This study investigated the impact of occasional saltwater intrusions (inversac in French) into
735 the karst hydrosystem of the Balaruc peninsula and provides an improved understanding of the
736 hydrodynamics and recovery of the aquifer from saltwater intrusions. Differences were
737 observed between the hydraulic and geochemical responses, both spatially and temporally. The
738 karst, thermal and marine water bodies within different compartments of the karst system
739 coexist within a very delicate equilibrium that is disturbed by the rapid intrusion of lagoon
740 waters during inversac events. While the hydraulic impact of such saltwater intrusions is
741 immediate and manifest over a distance of some 5 km within the hydrosystem, the geochemical
742 impact focused within a 1 km radius around the Vise spring but temporally persistent.
743 Geochemical tracers showed that the hydrosystem did not reach its pre-inversac reference state
744 20 months and 40 months after the occurrence of inversac of 6-months duration. The slow
745 geochemical recovery of the Balaruc peninsula karst system reflects the triple-porosity
746 character of the karst aquifer. Additionally, preliminary results suggested that the modification
747 of the groundwater chemistry is initiated by an interaction process with clay sediments and
748 organic matter during the saltwater intrusion event and possibly during the subsequent transfer
749 of seawater to the karst aquifer through the Miocene formation. This study demonstrates the
750 potential to couple physico-chemical, hydrogeological and isotopic data to understand the
751 complex inversac phenomenon and recognize preferential flowpaths during such events.

752 The results of this study support groundwater management across the Balaruc peninsula. The
753 triggering factors of the saltwater intrusions were highlighted as well as the conditions needed
754 for the saltwater intrusion to hydraulically impact the upgradient area, which is a major source
755 of drinking water supply. While the water quality of some of wells across the Balaruc peninsula
756 are strongly impacted by the inversac and retain a geochemical signature of the event, the
757 thermal wells located in the southern portion of the hydrosystem are not affected by inversac
758 events, suggesting hydraulic isolation from the remainder of the Balaruc peninsula.



759 **8. Data availability**

760 The geochemical and isotopic data are accessible at <https://doi.org/10.5281/zenodo.3893897>

761 **9. Supplement link**

762 The supplement related to this article is available online at

763 **10. Authors contribution**

764 BL, JLS and CL designed the study and data collection plan. MAP, JLS and BL conducted the
765 field work, collected the hydrogeological and geochemical data, and performed the data
766 analysis. MAP prepared the paper with contributions from RH and JLS. All authors reviewed
767 and edited the manuscript.

768 **11. Competing interests**

769 The authors declare that they have no conflict of interest

770 **12. Acknowledgements**

771 This work was funded by a FEDER-CPER grant (Agence de l'Eau, Balaruc-les-Bains, SMBT,
772 and BRGM) through the Dem'Eaux Thau project. Authors are thankful to the municipalities of
773 Balaruc les Bains and Pézenas for continuous support during the 2018 field work. Thanks are
774 due to Franck Bujaldon (city of Pézenas), Ludovic Sarrou (Thermal spa, Balaruc les Bains),
775 Nathalie Masscheleyn (Balaruc les Bains municipality), David Mimard (Suez) and Vincent
776 Durand (Antéa) for granting access to the thermal boreholes, karst springs and piezometers. We
777 are thankful to Jean-Gilbert Muller from President Electronics for providing access to the
778 Ambressac spring. Gilles Lorente and Kevin Buttaro (Syndicat Mixte du Bassin de Thau) are
779 thanked for their technical support during the March 2018 field campaign. We also
780 acknowledge Nicolas Patris (HydroSciences Montpellier) for his help and useful discussion on
781 stable isotopes. Remi Freydier (HydroSciences Montpellier) and graduate student Hikma
782 Kassime are also thanked for their valuable contribution on the B isotopic analyses. We thank
783 Russell Harmon (North Carolina State University) for a thorough review of an earlier version
784 of the manuscript.

785

786 **13. References**



- 787 Aggarwal and Palmer 1995 Boron isotope analysis. A review. *Analyst*, 1995, 120, 1301-1307.
788 DOI: 10.1039/AN9952001301
- 789 Aggarwal, J.K., Mezger, K., Pernicka, E., Meixner, A., 2004. The effect of instrumental mass
790 bias on d11B measurements: a comparison between thermal ionisation mass spectrometry and
791 multiple-collector ICP-MS. *Internat. J. Mass Spectrom.* 232, 259-263.
- 792 Albéric, P.: River backflooding into a karst resurgence (Loiret, France), *Journal of Hydrology*,
793 286(1-4), 194-202, 2004.
- 794 Aquilina, L., Deluchat, V., Brach, M., Bakalowicz, M., Le Strat, P. and Giraud, F: Etude
795 géochimique des eaux souterraines autour du bassin de Thau. Rap. BRGM R39530, 58 p., 15
796 fig., 4 tabl., 2 annexes., 1997.
- 797 Aquilina, L., Ladouche, B., Dörfliger, N., Seidel, J. L., Bakalowicz, M., Dupuy, C. and Le Strat,
798 P.: Origin, evolution and residence time of saline thermal fluids (Balaruc springs, southern
799 France): implications for fluid transfer across the continental shelf, *Chemical Geology*, 192(1-
800 2), 1-21, 2002.
- 801 Aquilina, L., Ladouche, B., Doerfliger, N. and Bakalowicz, M.: Deep water circulation,
802 residence time, and chemistry in a karst complex, *Groundwater*, 41(6), 790-805, 2003.
- 803 Arfib, B. and Gilli, E: Karst côtier et sources sous-marines-fonctionnement et exploitation.,
804 2010.
- 805 Arthaud, F. and Laurent, P: Contraintes, déformation et déplacement dans l'avant-pays Nord-
806 pyrénéen du Languedoc méditerranéen, *Geodinamica Acta*, 8(3), 142-157,
807 doi:10.1080/09853111.1995.11105386, 1995.
- 808 Arthaud, F. and Seguret, M: Les structures pyrénéennes du Languedoc et du Golfe du Lion
809 (Sud de la France), *Bulletin de la Société Géologique de France*, S7-XXIII(1), 51-63,
810 doi:10.2113/gssgfbull.S7-XXIII.1.51, 1981.
- 811 Arthaud, F., Mégard, F. and Séguret, M: Cadre tectonique de quelques bassins sédimentaires,
812 *Bulletin du Centre de Recherche, d'Exploration et de Production, Elf-Aquitaine.*, 1, 147-188,
813 1977.
- 814 Bakalowicz, M.: Karst at depth below the sea level around the Mediterranean due to the
815 Messinian crisis of salinity. Hydrogeological consequences and issues, *Geologica Belgica*,
816 2014.
- 817 Baudrimont, A. F. and Dubois, P: Un bassin mésogéen du domaine péri-alpin: le Sud-Est de la
818 France, *Bulletin Centre Recherche Exploration Production Elf-Aquitaine*, 262-308, 1977.
- 819 Benedicto, A., Labaume, P., Séguret, M. and Séranne, M.: Low-angle crustal ramp and basin
820 geometry in the Gulf of Lion passive margin: Oligocene-aquitainian Vistrenque graben, SE
821 France, *Tectonics*, 15(6), 1192-1212, doi:10.1029/96TC01097, 1996.
- 822 Choukroune, P. and Mattauer, M: Tectonique des plaques et Pyrénées: sur le fonctionnement
823 de la faille transformante nord-pyrénéenne; comparaison avec des modèles actuels, *Bulletin de*
824 *la Société Géologique de France*, 7(5), 689-700, 1978.



- 825 Choukroune, P., Seguret, M. and Galdeano, A.: Caractéristiques et évolution structurale des
826 Pyrénées; un modèle de relations entre zone orogénique et mouvement des plaques, Bulletin de
827 la Société Géologique de France, S7-XV(5–6), 600–611, doi:10.2113/gssgfbull.S7-XV.5-
828 6.600, 1973.
- 829 Chu, Y., Tournoud, M. G., Salles, C., Got, P., Perrin, J.-L., Rodier, C., Caro, A. and
830 Troussellier, M.: Spatial and temporal dynamics of bacterial contamination in South France
831 coastal rivers: focus on in-stream processes during low flows and floods, Hydrological
832 processes, 28(8), 3300–3313, 2014.
- 833 Clauzon, G: Le canyon messinien du Rhône; une preuve décisive du “desiccated deep-basin
834 model” (Hsue, Cita and Ryan, 1973), Bulletin de la Société Géologique de France, S7-XXIV(3),
835 597–610, doi:10.2113/gssgfbull.S7-XXIV.3.597, 1982.
- 836 Combes, J.-P: Typologie, cadre géodynamique des bauxites téthysiennes, Geodynamica Acta,
837 4, 91–109, 1990.
- 838 Debrand-Passard, S: Synthèse géologique du Sud-Est de la France - Stratigraphie et
839 paléogéographie., 1984.
- 840 Doerfliger, N., Ladouche, B., Bakalowicz, M., J.-L. Pinault and Chemin, P: Étude du pourtour
841 est de l’étang de Thau, phase II. Synthèse générale. Volume 4. BRGM/RP-50789-
842 FR, 71 p., 34 fig., 3 tabl., 2 photos., 2001.
- 843 Drogue, C. and Bidaux, P.: Simultaneous outflow of fresh water and inflow of sea water in a
844 coastal spring, Nature, 322(6077), 361–363, doi:10.1038/322361a0, 1986.
- 845 Faure, G.: Principles of isotope geology, Second ed Wiley, New-York. 588 p., 1986.
- 846 Fleury, P: Sources sous-marines et aquifères karstiques côtiers méditerranéens :
847 Fonctionnement et caractérisation., 2005.
- 848 Fleury, P., Bakalowicz, M. and de Marsily, G.: Submarine springs and coastal karst aquifers: a
849 review, Journal of Hydrology, 339(1–2), 79–92, 2007.
- 850 Gèse, B: Les mésaventures des sources de l’Estavelle et de l’Inversac en Languedoc
851 méditerranéen, Int. J. Speleol, 16, 101–109, 1987.
- 852 Guerrot, C., Millot, R., Robert, M. and Négrel, P.: Accurate and High-Precision Determination
853 of Boron Isotopic Ratios at Low Concentration by MC-ICP-MS (Neptune), Geostandards and
854 Geoanalytical Research, 35(2), 275–284, doi:10.1111/j.1751-908X.2010.00073.x, 2011.
- 855 Han, D., Post, V. E. and Song, X.: Groundwater salinization processes and reversibility of
856 seawater intrusion in coastal carbonate aquifers, Journal of Hydrology, 531, 1067–1080, 2015.
- 857 Hemelsdaël, R., Séranne M., Jacob T., Husson E., Courrioux G., Caritg S., Ballas G. (in prep)
858 Structural style of the Languedoc Pyrenean thrust belt in relation with the polyphased history
859 of the western Gulf of Lion margin, SE France. To be submitted in Earth Sciences Bulletin
860
- 861 Hershey J.P., Fernandez M., Milne P.J., Millero F.J. (1986) The ionization of boric acid in
862 NaCl, Na-Ca-Cl and Na-Mg-Cl solutions at 25°C. Geochim. Cosmochim. Acta, 50: 143-148



- 863 Hsu, K. J.: The origin of the Mediterranean evaporites, edited by W. B. F. Ryan and K. J. Hsu,
864 Initial reports of the deep sea drilling project, 13, 1203–1231, 1973.
- 865 Kakihana H., Kotaka M., Satoh S., Nomura M., Okamoto M. (1977) Fundamental studies on
866 the ion-exchange separation of boron isotopes. *Bull. Chem. Soc. Japan.*, 50: 158-163.
- 867 Johannesson, K. H., Stetzenbach, K. J. and Hodge, V. F.: Rare earth elements as geochemical
868 tracers of regional groundwater mixing, *Geochimica et Cosmochimica Acta*, 61(17), 3605–
869 3618, doi:10.1016/S0016-7037(97)00177-4, 1997.
- 870 Joigneaux, E., Albéric, P., Pauwels, H., Pagé, C., Terray, L., Bruand, A., 2011. Impact of
871 climate change on groundwater point discharge: backflooding of karstic springs (Loiret,
872 France). *Hydrol. Earth Syst. Sci.* 15, 2459–2470. <https://doi.org/10.5194/hess-15-2459-2011>
- 873
- 874 La Jeunesse, I., Cirelli, C., Sellami, H., Aubin, D., Deidda, R. and Baghdadi, N.: Is the
875 governance of the Thau coastal lagoon ready to face climate change impacts?, *Ocean & Coastal*
876 *Management*, 118, 234–246, 2015.
- 877 Lacombe, O. and Jolivet, L.: Structural and kinematic relationships between Corsica and the
878 Pyrenees-Provence domain at the time of the Pyrenean orogeny, *Tectonics*, 24(1), 1–20,
879 doi:10.1029/2004TC001673, 2005.
- 880 Ladouche, B. and Lamotte, C: Inversac de la source sous-marine de la Vise en 2014 :
881 Recueil et analyse des données disponibles. Rapport final. BRGM/RP - 64812 - FR 82 p., 56
882 ill. ., 2015.
- 883 Ladouche, B., Aquilina, L., Cubizoles, J. and Négrel, P.: Rainfall chemistry in the south of
884 France (Hérault, 1996-1997), in *Mineralogical Magazine*, 8th Annual VM Goldschmidt
885 Conference, vol. 30, pp. 842–843., 1998.
- 886 Ladouche, B., Doerfliger, N., Bakalowicz, M. and avec la collaboration de J. Cubizolles:
887 Étude du pourtour est de l'étang de Thau. Phase II. Caractérisation hydrochimique des
888 réservoirs souterrains karstiques et thermaux. Volume 3. BRGM/RP-50788-FR, 9 p., 20
889 fig., 5 tabl., 5 ann., 2001.
- 890 Ladouche, B., Millot, R., Guerrot, C. and Lamotte, C: Caractérisation géochimique de
891 l'aquifère hydrothermal de Balaruc-les-Bains lors d'un épisode d'inversac, in *Dix-huitièmes*
892 *jours techniques du Comité Français d'Hydrogéologie de l'Association Internationale des*
893 *Hydrogéologues.* ” Ressources et gestion des aquifères littoraux. Cassis 2012. ”, pp. 141–149,
894 Cassis, France. [online] Available from: <https://hal-brgm.archives-ouvertes.fr/hal-00680642>
895 (Accessed 16 August 2018), 2012.
- 896 Ladouche B., Lamotte C., Hemelsdael R., Pétré M.A., Dewandel B., Léonardi V., Seidel J.L.,
897 Séranne M. (2019) - Dem'Eaux Thau - Synthèse et valorisation préliminaire des données sur
898 l'hydrosystème de Thau (34). Rapport final. BRGM/RP-68483-FR, 313 p., 133 fig., 6 tab., 6
899 ann.
- 900 Maerten, L. and Séranne, M: Extensional tectonics of the Oligo-Miocene Hérault Basin (S
901 France), Gulf of Lion margin, *Bulletin de la Société Géologique de France*, 166(6), 739–749,
902 1995.



- 903 Martin, J.B. and Screamon, E.J., 2001, Exchange of matrix and conduit water with examples
904 from the Floridan aquifer, in E.L. Kuniansky (ed.), U.S. Geological Survey Karst Interest Group
905 Proceedings, Water-Resources Investigations Report 01-4011, p.38-44.
- 906 Palmer, A.N., 1999, Introduction, in A.N. Palmer, M.V. Palmer, and I.D. Sasowsky (eds.),
907 Karst Modeling: Charles Town, West Virginia, Karst Waters Institute Special Publication 5, p
908 1-9.
- 909 Paloc and Bonnet 1969, Definition de la structure géologique profonde du bassin de
910 Montbazin-Gigean. BRGM/69 SGL 207 LRO
- 911 Pinault, J.-L., Dörfliger, N., Ladouche, B. and Bakalowicz, M.: Characterizing a coastal karst
912 aquifer using an inverse modeling approach: The saline springs of Thau, southern France, Water
913 Resources Research, 40(8), 2004.
- 914 Ryan, W. B. F.: Quantitative evaluation of the depth of the western Mediterranean before,
915 during and after the Late Miocene salinity crisis, *Sedimentology*, 23(6), 791–813,
916 doi:10.1111/j.1365-3091.1976.tb00109.x, 1976.
- 917 Séranne, M.: The Gulf of Lion continental margin (NW Mediterranean) revisited by IBS: an
918 overview, *Geological Society, London, Special Publications*, 156(1), 15–36,
919 doi:10.1144/gsl.sp.1999.156.01.03, 1999.
- 920 Stieglitz, T. C., van Beek, P., Souhaut, M. and Cook, P. G.: Karstic groundwater discharge and
921 seawater recirculation through sediments in shallow coastal Mediterranean lagoons, determined
922 from water, salt and radon budgets, *Marine Chemistry*, 156, 73–84, 2013.
- 923 Taylor, S. and McLennan, S.: *The continental crust: its composition and evolution.*, Blackwell
924 Scientific Publications, Oxford., 1985.
- 925 Thaler, L. : Premiers résultats d'une recherche systématique des dents de rongeurs, par lavage
926 de marnes de l'Oligocène, en Bas-Languedoc, *Comptes Rendus Sommaires de la Société
927 Géologique de France*, 10, 315–315, 1962.
- 928 Tweed, S. O., Weaver, T. R., Cartwright, I. and Schaefer, B.: Behavior of rare earth elements
929 in groundwater during flow and mixing in fractured rock aquifers: An example from the
930 Dandenong Ranges, southeast Australia, *Chemical Geology*, 234(3), 291–307,
931 doi:10.1016/j.chemgeo.2006.05.006, 2006.
- 932 Zhan, Y., Guo, H. and Xing, L.: Characteristics of Rare Earth Elements in Groundwaters along
933 the Flow Path in the North China Plain, *Procedia Earth and Planetary Science*, 7, 940–943,
934 doi:10.1016/j.proeps.2013.03.173, 2013.

935